Biosensors and Bioelectronics 47 (2013) 213–217

Contents lists available at SciVerse ScienceDirect

Biosensors and Bioelectronics

journal homepage: www.elsevier.com/locate/bios

Short communication

Conditions for efficient on-chip magnetic bead detection via magnetoresistive sensors

E. Albisetti [a,b,*], D. Petti [a], M. Cantoni [a], F. Damin [b], A. Torti [a], M. Chiari [b], R. Bertacco [a]

[a] L-NESS, Dipartimento di Fisica, Politecnico di Milano, Via Anzani 42, 22100 Como, Italy
[b] Istituto di Chimica del Riconoscimento Molecolare, CNR, Via Mario Bianco 9, 20131 Milan, Italy

ARTICLE INFO

Article history:
Received 6 December 2012
Received in revised form
5 March 2013
Accepted 6 March 2013
Available online 22 March 2013

Keywords:
Magnetic biosensor
Magnetic tunneling junction
Magnetic bead

ABSTRACT

A commonly used figure of merit of magnetoresistive sensors employed to detect magnetic beads labeling biomolecules in lab-on-chip applications is the sensor sensitivity (S_0) to external magnetic fields in the linear region of the sensor. In this paper we show that, in case of lock-in detection and bead excitation by a small AC magnetic field, S_0 is not the good figure of merit to optimize. Indeed, the highest sensitivity to the magnetic beads is achieved biasing the sensor in the region of its characteristics where the product between the DC bias field and the second derivative of the resistance with respect to the magnetic field is maximum. The validity of this criterion, derived from a phenomenological model of bead detection, is proved in case of magnetic tunneling junction sensors detecting magnetic beads with 250 nm diameter. This work paves the way to the development of a new generation of sensors properly designed to maximize the bead sensitivity.

1. Introduction

Magnetoresistive sensors embedded in biochip platforms have received considerable interest in the last few years, essentially because they allow for the detection of low concentrations of biological entities labeled by magnetic beads. Giant magnetoresistance (GMR), tunneling magnetoresistance (TMR), anisotropic magnetoresistance (AMR) and Planar Hall Effect (PHE) sensors have been successfully used for detecting single magnetic beads labeling cells or single molecules (Chaves et al., 2011; Vavassori et al., 2008). Biomolecular detection of analyte concentrations down to the zeptomolar range (Martins et al., 2009; Gaster et al., 2011) has been achieved without biochemical amplification. This high sensitivity essentially relies on two factors: (i) the minimization of the sensor noise and (ii) the maximization of the sensor magnetic sensitivity, which is generally expressed as the maximum percentage variation of the sensor resistance (R) per unit change of the external field (H): $S_0=(R\mu_0)^{-1}(\mathrm{d}R/\mathrm{d}H)$. Values of S_0 as high as 70%/mT have been reported ((Wiśniowski et al., 2008) for TMR sensors used in bio-molecular recognition applications, where the latter value represents the maximum of the derivative in the linear portion of the $R(H)$ characteristics. In practice, however, these sensors are not used in the linear regime, where S_0 is maximum, but with an external bias magnetic field shifting the operation point in the non-linear zone of the $R(H)$ curve, where S_0 is sizeably smaller (Wang et al., 2005; Cardoso, 2011). The reasons for such a counterintuitive choice have not been fully clarified so far. The compensation of the stray fields coming from the free and pinned layers of the sensors, as well as the need for a DC field to magnetize the beads have been invoked to explain the need for this magnetic bias of the sensors (Ferreira et al., 2005) but a comprehensive and general explanation is still missing. In this work we present a theoretical model describing the operation of magnetoresistive sensors for the AC detection of magnetic beads, i.e. by exciting the beads with a small AC magnetic field and detecting the corresponding signal with a lock-in amplifier. As a general criterion for efficient bead detection we found that the sensors must be operated not in the linear regime, but properly biased, via an external DC magnetic field, at a point of their characteristics where the product between the DC bias field and the second derivative of the $R(H)$ curve is maximum. The validity of our approach is demonstrated using MgO-based TMR sensors integrated in a microfluidic cell, whose sensitivity to magnetic bead sedimentation has been investigated as a function of the external DC bias field. This work sheds light on the choice of the best operating working point of magnetoresistive sensors for biochip applications, possibly paving the way to the development of new architectures for magnetoresistive sensors particularly suitable for efficient bead detection.

2. Materials and methods

Magnetic Tunneling Junctions (MTJ) stacks with the structure (thicknesses in nm from now on) Si/SiO_2(1000)/Ta(5)/Ru(18)/Ta

* Corresponding author at: Department of Physics, Politecnico di Milano, L-NESS Laboratory, Via Anzani 42, 22100 Como, Italy. Tel.: +39 031 332 7308 (office), +39 031 332 7618 (Lab); fax: +39 031 332 7617.
E-mail address: edoardo.albisetti@mail.polimi.it (E. Albisetti).

0956-5663/$ - see front matter © 2013 Elsevier B.V. All rights reserved.
http://dx.doi.org/10.1016/j.bios.2013.03.016

(3)/$Ir_{22}Mn_{78}$(20)/$Co_{50}Fe_{50}$(2)/Ru(1.1)/$Co_{40}Fe_{40}B_{20}$(3)/MgO(2)/ $Co_{40}Fe_{40}B_{20}$(1)/Ru(5)/Ta(5), were deposited by magnetron sputtering in a AJA Orion8 system with a base pressure of 2×10^{-9} Torr. CoFe and MgO layers were deposited in RF mode, while all other layers were deposited in DC mode.

After the deposition of the stack, arrays of 8 MTJ sensors (Fig. 1A) were fabricated using optical lithography and the same layout as in Donolato et al. (2011). The junction areas were defined by ion milling in the form of rectangles, $2.5\times120\ \mu m^2$ wide, where the shorter side is parallel to the easy axis of the pinned bottom reference layer, oriented along the *y*-axis in Fig. 1B. After e-beam evaporation of Cr(7)/Au(300) contacts, the samples were annealed at 330 °C at a pressure of 10^{-6} Torr for 1 h in a magnetic field of 400 mT applied along the positive *y*-direction. Then, a 200 nm thick SiO_2 layer was deposited in RF mode from a SiO_2 target to electrically insulate the sensor stack and protect it against fluids dispensed on the chip via the microfluidic apparatus. The latter consists in a click-on microfluidic system made of a chip holder in Polycarbonate (PC), on top of which a microfluidic chamber is defined via a Polydimethylsiloxane (PDMS) gasket and a PC cover with the retractable tips for contacting the bottom and top electrodes of each sensor. In Fig. 1C the sensor transfer curve $R(H)$ for a field applied in the *y*-direction is reported. The curve displays a tunneling magnetoresistance of 50% and a low-field sensitivity $S_0=(R\mu_0)^{-1}(dR/dH)=12\%/mT$ in the linear region. This sensitivity results from the combined effect of the shape anisotropy (Lu et al., 1997) and the superparamagnetic behavior of the top FeCoB layer (Wiśniowski et al., 2008), leading to an easy axis of the top free layer perpendicularly aligned to that of the reference layer and to negligible hysteresis. The shift of the characteristic towards negative fields can instead be attributed to Néel or dipolar coupling between the top and bottom layers of the tunneling junction. The scheme of the circuit used for detecting the AC signal in response to the applied AC magnetic field is reported in the inset of Fig. 1C. To improve the sensor sensitivity and minimize the $1/f$ noise (Han et al., 2006), the voltage applied to the series of a fixed resistance ($r=1$ kΩ) and of the sensor resistance $R(H)$ is modulated at a frequency $f_1=51$ kHz ($V_{in}(t)=V_s\cos(2\pi f_1 t)$, $V_s=250$ mV), while an external magnetic field H_e is applied parallel to the sensing axis, which corresponds to the *y*-direction in Fig. 1B. H_e is the sum of two contributions: a bias field H_{DC} and a small oscillating field $H_{AC}=h\cos(2\pi f_2 t)$ used for exciting the beads, where $h=0.5$ mT and $f_2=39$ Hz. Thanks to this double modulation, the response to H_{AC}, eventually depending on the concentration of beads above the sensor, appears in the output voltage (V_{out}) as a component at the frequency ($f_1\pm f_2$), which can be easily extracted via a lock-in amplifier. The amplitude of the small oscillating field $h=0.5$ mT has been chosen as the best compromise between two needs: (i) maximizing the excitation field of the beads and (ii) keeping its amplitude as small as possible in order to fully exploit the local non-linearity of the $R(H)$ sensor characteristics.

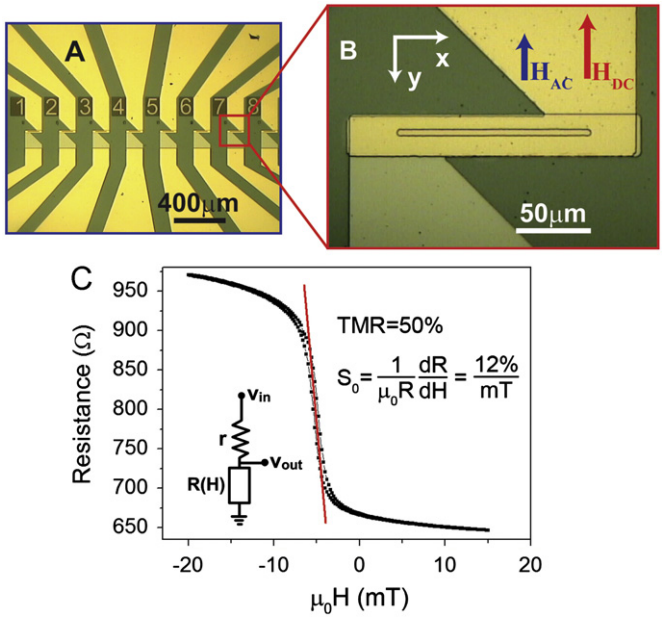

Fig. 1. (A) Optical image of the layout of the chip with 8 MTJs sensors. (B) Zoom on a single sensor showing the geometry of the applied magnetic fields. (C) Sensor resistance $R(H)$ measured applying a 10 mV voltage across the junction. In the inset the sketch of the circuit used for AC detection is shown. (For interpretation of the references to color in this figure, the reader is referred to the web version of this article.)

3. Results and discussion

To investigate the sensitivity to the bead concentration in various operating conditions we monitored the output voltage during bead sedimentation. Upon injecting in the cell, at a rate of 150 μl/min, an aqueous suspension with fixed concentration (~4.9×10^{10} beads/ml) of Micromod nanomag® -D streptavidin nanoparticles with 250 nm diameter, we stop the syringe pump and wait for 15 min, allowing for a full sedimentation of the beads. Then we wash out the bead suspension with de-ionized (DI) water at a rate of 450 μl/min, till the signal recovers the initial baseline. The signal acquired during sedimentation and subsequent washing is shown in Fig. 2A and B for two different values of the bias field, namely −5.1 mT and −6.0 mT. Interestingly enough, the signal variation ΔS upon bead sedimentation changes sign for such a relatively small variation of the bias fields. In Fig. 2C we plot with red dots the ΔS values measured for different DC bias, normalized to the maximum value obtained in these experiments (see Table 1). Apart from the null signal at high positive and negative fields, where the sensing layer is in saturation, the oscillating behavior of the sensitivity to beads seen in Fig. 2C is particularly critical for the device operation. In fact, even a minor shift of the bias field from −5.0 mT, corresponding to the maximum bead sensitivity, to −5.8 mT, determines the complete suppression of the sensitivity to magnetic beads. Noteworthy, −5.8 mT corresponds to the point of the sensor characteristic where the sensor sensitivity to external magnetic fields (S_0) is maximum, pointing out that S_0 is definitely not a good figure of merit in case of magnetoresistive sensors employed for bead detection purposes.

In order to shed light on the physical mechanisms giving rise to such a behavior and find out a general criterion for correctly choosing the bias field, we developed a phenomenological model of bead detection. For small h values, as compared with the width of the linear regime of the $R(H)$ characteristics, the AC magnetic field used for exciting the beads can be considered as a perturbation superposed to the DC bias field so that, without beads above the sensor, we can write:

$$R(H_{DC}+H_{AC})\approx R(H_{DC})+\left.\frac{dR}{dH}\right|_{H_{DC}} h\cos(2\pi f_2 t). \quad (1)$$

The average DC and AC stray fields produced by the beads on the sensor free layer are instead $H_{bDC}=\alpha_{DC}H_{DC}$ and $H_{bAC}=\alpha_{AC}H_{AC}$ (see Supplementary data for the discussion about the impact of demagnetizing fields coming from the sensor ferromagnetic layers and about the magnetic interaction between the two layers via Néel coupling). Here, the linear bead response is described by the coefficient $\alpha=\beta\chi V_b n$, where χ is the magnetic susceptibility of the beads (AC or DC), V_b their volume, n the number of beads per unit volume and β is a geometrical factor which depends on the beads

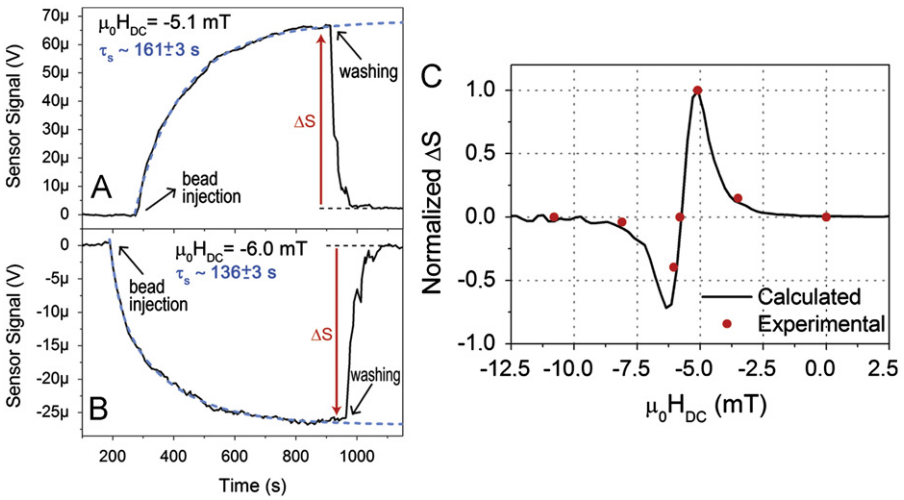

Fig. 2. (A,B) Bead sedimentation for different bias magnetic field H_{DC}; the blue dashed line is an exponential fit of the signal from which the sedimentation time constant τ_s is extracted. (C) ΔS signal normalized to its highest value (red dots) as a function of the applied magnetic field H_{DC}; the black line is a fit performed accordingly to Eq. (5). (For interpretation of the references to color in this figure legend, the reader is referred to the web version of this article.)

Table 1
α_{DC} parameter, sedimentation signal (ΔS), baseline noise (N), signal to noise ratio ($|\Delta S|/N$) and sedimentation time constant (τ_s) as a function of the applied magnetic field H_{DC}.

$\mu_0 H_{DC}$(mT)	α_{DC}	ΔS (μV)	N (μV)	$\lvert\Delta S\rvert/N$	τ_s (s)
0	–	0	–	–	–
−3.0	-1.45×10^{-2}	10	4.59×10^{-2}	218	224 ± 1
−5.1	-5.9×10^{-3}	66	2.04×10^{-1}	323	161 ± 3
−5.8	–	0	1.58×10^{-1}	–	–
−6.0	-4.85×10^{-3}	−25	1.60×10^{-1}	156	136 ± 3
−8.1	-1.12×10^{-2}	−2.7	3.99×10^{-2}	68	22 ± 1
−10	–	0	–	–	–

size and distribution over the sensor area (Donolato et al., 2011; Hansen et al., 2010). The stray field generated by magnetic beads then adds up to the external fields leading to:

$$R(H_{DC}+H_{AC})\approx R(H_{DC}(1+\alpha_{DC}))+\frac{dR}{dH}\Big|_{(1+\alpha_{DC})} h(1+\alpha_{AC})\cos(2\pi f_2 t) \quad (2)$$

The sensor output voltage can then be written as:

$$V_{out}=V_s\left(\frac{R(H_{DC}(1+\alpha_{DC}))}{r+R(H_{DC}(1+\alpha_{DC}))}\cos(2\pi f_1 t)+\frac{1}{2}\frac{dR}{dH}h(1+\alpha_{AC})\times\frac{r}{(r+R(H_{DC}(1+\alpha_{DC})))^2}(\cos(2\pi(f_1-f_2)t)+\cos(2\pi(f_1+f_2)t))\right) \quad (3)$$

The normalized signal S_v, demodulated by the lock-in at a frequency (f_1+f_2) results:

$$S_v=\frac{V_{out}}{V_s}=\left(\frac{1}{2}\frac{dR}{dH}\Big|_{H_{DC}(1+\alpha_{DC})} h(1+\alpha_{AC})\frac{r}{(r+R(H_{DC}(1+\alpha_{DC})))^2}\right) \quad (4)$$

Finally, the net signal ΔS (see Fig. 2A and B) due to the sedimentation of the beads on the sensor surface can be calculated within the approximation $|\alpha_{DC}|\ll1$ (See Supplementary Information for details), leading to:

$$\Delta S=S_v\Big|_{beads}-S_v\Big|_{plain}=\frac{1}{2}\frac{r}{(r+R(H_{DC}))^2}h\alpha_{AC}\left(\frac{dR}{dH}\Big|_{H_{DC}}+\frac{d^2R}{dH^2}\Big|_{H_{DC}}H_{DC}\right) \quad (5)$$

According to this expression, ΔS is not simply proportional to α_{AC}, but also to the sum of $\frac{dR}{dH}\Big|_{H_{DC}}$ and $\left(\frac{d^2R}{dH^2}\Big|_{H_{DC}}\cdot H_{DC}\right)$. The presence

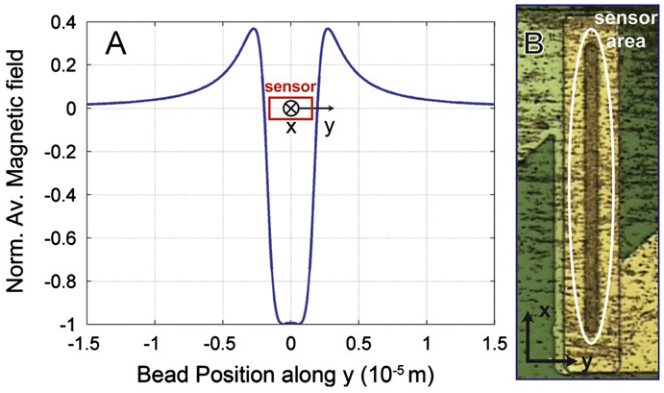

Fig. 3. (A) Average magnetic field H_{DC} produced by a single bead on the sensor as a function of the bead position along the y-direction with respect to the sensor. (B) Optical image of the sensor area after sedimentation: the bead distribution is concentrated upon the sensor area due to focusing action of the sensor stray field. (For interpretation of the references to color in this figure, the reader is referred to the web version of this article.)

of the latter term explains why for the same bead concentration and distribution above the sensor resulting upon complete sedimentation (i.e. for similar values of the parameter α_{AC}) we can find different values of ΔS and even an inversion of its sign for different bias fields H_{DC}, as previously discussed. This is because the second derivative in the last term of Eq. (5) changes sign when sweeping the bias field. It is largely negative for −6.0 mT and becomes positive for −5.1 mT, while for a critical intermediate field a perfect compensation of the two terms containing the first and second derivative in the bracket takes place, eventually leading to $\Delta S=0$. The soundness and reliability of our interpretation is confirmed by the nice fit (black continuous line in Fig. 2C) of the experimental values for the normalized bead signal ΔS reported in Fig. 2C, that we obtained using Eq. (5) with $\alpha_{AC}=-3.73\times10^{-3}$ Furthermore, the fitting procedure gives rise to a negative value of α and β, consistent with the simulations reported in Fig. 3. Following previous works (Donolato et al., 2011; Hansen et al., 2010), we calculated the average magnetic field on the sensor area from a single bead in suspension above the sensor, magnetized by the field in the y-direction as a function of the position of the bead itself. For a monolayer of beads, located 800 nm above the sensor (this is the overall thickness of the capping and contact layers of our devices),

we can estimate the sign of β, and hence of α, by integrating the contributions arising from the single beads. In Fig. 3A, the average H_{DC} generated by a bead on the sensor is plotted as a function of the bead position along the y-axis, keeping the bead position along the x-axis fixed in the center of the sensor. The values are normalized to the modulus of the maximum average field H_{MAX}. The average field is negative when the bead is above the sensor area and positive when it is outside the sensor area. For a homogeneous bead distribution, the positive and negative contributions cancel each other, implying that in this case a monolayer of beads would not give a detectable sensor response. As shown in the optical image of Fig. 3B, however, after sedimentation, beads are mainly concentrated above the sensor area due to the focusing action of the sensor stray field. In fact the sensor area in Fig. 3B is brown due to the bead accumulation, at variance with the case of absence of beads reported in Fig. 1B, where the sensor and the surrounding area are the same color, i.e. pale brown. As a consequence, the overall sign of H_{DC}, and hence of α, is negative, in agreement with the values of alpha used in the fit. Note also that the first term in the brackets of Eq. (5), which coincides with the first derivative, is typically smaller than the last term, containing the second derivative (see Supplementary Information). As a result, the entity of the first derivative essentially determines the critical bias field leading to zero sensitivity. To summarize, from our analysis it turns out that the maximum variation of the sensor signal due to the beads (ΔS) can be achieved not in the linear region of the sensor characteristics, but at some bias H_{DC} where the second derivative, multiplied by the bias field itself, is maximum. The above criterion for the choice of the best DC bias can be easily understood with reference to the mechanism used for AC detection. As pointed out in Eq. (4), the sensor output upon the lock-in demodulation is proportional to the first derivative of the sensor characteristic. Therefore, we can expect an increase of ΔS in a working point where the AC stray field from the beads can produce a significant change in the first derivative, i.e. where the second derivative is large. This is exactly the meaning of the second term in the brackets of Eq. (5), where the presence of the factor H_{DC} essentially indicates that a static field is required in order to magnetize the beads whose corresponding DC stray field can then shift the working point of the sensor. Note that this is different from the case of DC detection of beads already discussed by Wang et al. (2005). As a matter of fact, in the latter paper, the authors show an oscillating behavior of the bead sensitivity vs. DC bias field very similar to the one shown in Fig. 2C. In case of perfectly symmetric sensor characteristics, without shift due to magnetic coupling between layers, they correctly explain the maxima for non-zero bias as the result of the compromise between the sensor sensitivity and the need for non-zero bias field in order to get the beads magnetized. However, the case of AC detection is quite different, because a non-null bead signal can be achieved also without DC net bias field, as there is in any case an oscillating AC field exciting the beads and then producing a signal detectable by the lock-in. Indeed, Eq. (5) points out that in case $H_{DC}=0$ a net bead signal is still present. Our model clarifies that, in the AC detection mode, an external DC bias is needed not simply to magnetize the beads, but essentially in order to drive the sensor in a highly non-linear region of its characteristic where the sensitivity to the beads is maximum.

The characteristic sedimentation time (τ_s), the bead signal (ΔS), the root mean square noise of our base-line signal (N) and the signal to noise ratio ($|\Delta S|/N$) for each DC bias field tested in our experiment are reported in Table 1. As expected, the sedimentation time monotonically decreases when increasing the field H_{DC}, at variance with the sensor sensitivity to beads which presents an oscillating behavior, thus indicating that spurious effect coming from the different focusing of beads on top of the sensor due to the stray field play a minor role. The estimated values of the coefficient α_{DC} (see Supplementary Information for details), describing the overall capability of the beads to produce a change of the magnetic field on the sensing layer upon complete sedimentation, show indeed minor modifications as a function of the bias field. Noteworthy, α_{DC} is minimum where we found the maximum sensitivity to beads, clearly ruling out the possibility that the best operating condition corresponds to the optimum focusing of the beads during sedimentation. The stray field of the top CoFeB free layer can indeed have some impact on the determination of the best operating conditions. A more detailed analysis reported in the Supplementary Information shows that the main effect could be only a minor shift of the position of the maxima in the curve of Fig. 2C by less than 1 mT.

Let us finally discuss the influence of the bias on the signal to noise ratio, which is the ultimate figure of merit to be optimized. From Table 1 it is evident that the highest level of noise N, defined here as the standard deviation of the signal baseline before sedimentation, is found in the linear region of the sensor, while it decreases approaching the magnetic saturation of the free electrode, where magnetic fluctuations are suppressed. This implies that the signal to noise ratio, defined as the ratio $|\Delta S|/N$, has even more pronounced maxima in correspondence to the maxima of ΔS than ΔS itself. The proposed criterion for the choice of the best operating conditions of the sensors thus allows also to maximize the signal to noise ratio.

The above criterion was successfully applied for maximizing the bead sensitivity of the sensors in biomolecular recognition detection experiments. The surface of the sensor was coated with a copolymer of dimethylacrylamide (DMA), N-acryloyloxysuccinimide (NAS) and 3-(trimethoxysilyl) propyl methacrylate (MAPS), copoly (DMA–MAPS–NAS), which provides reactive groups suitable for immobilization of amino modified oligonucleotide probe molecules and, at the same time, prevents non-specific adsorption of biological fluids components. The copolymer was synthesized and characterized in previous works (Pirri et al., 2004; Sola et al., 2012). According to the post-hybridization detection method, first a 23- mer synthetic probe oligonucleotide with the following sequence: 5′-GCCCACCTATAAGG-TAAAAGTGA-3′, modified at the 5′ end with a C_6 amino linker, was spotted over the whole sensor area. A control 23- mer synthetic oligonucleotide with the following sequence: 5′-TCACTTTTACCTTA-TAGGTGGGC-3′, modified at the 5′ end with a C_6 amino linker, was spotted over the area of a reference sensor on the same chip. The oligonucleotides were dissolved in 150 mM sodium phosphate buffer pH 8.5 at a final concentration of 10 μM and spotted using a non-contact microarray spotter SCENION sci-FLEXARRAYER S5 assembled with a 80 μm nozzle. Spot volume, temperature and humidity were 400 pL, 22 °C and 50% respectively. After binding the oligonucleotides overnight in the humid chamber, the excess of reactive groups on the sensor surface were blocked by a 30 min bath at 50 °C in 50 mM ethanolamine in 0.1 M TRIS/HCl at pH 9. The spotted and blocked sensors were then incubated with the oligonucleotide target of sequence 5′-TCACTTTTACCTTATAGGTGGGC-3′ labeled with biotin at the 5′ end. The target oligonucleotide was dissolved in a solution 1 μM of 2X SSC, 0.1% SDS and 0.2 mg/ml of BSA. The sensor chip, assembled in the above mentioned microfluidic cell, was flushed with 3 mg/ml solution of 250 nm diameter Micromod Nanomag-D® streptavidin-coated magnetic beads dispersed in PB-Tween. After about 25 min, a washing solution (PB-Tween solution) was flushed in the microchamber to remove the unbound beads from the sensor surface. In Fig. 4 the sensor output vs. time during the bioassay with 1 μM target DNA concentration is shown. The initial decrease of the signal is related to the sedimentation of beads in static conditions, after insertion in the microfluidic chamber. Washing removes all the beads non-specifically bound on the surface due to the strong streptavidin–biotin affinity. The difference between the two base lines in the sensor, before bead insertion and after the washing steps,

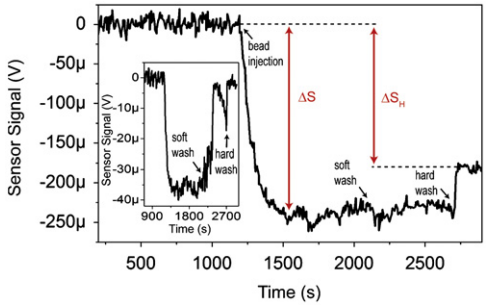

Fig. 4. Sensor output during a biomolecular recognition experiment with a DNA target concentration of 1 μM. The downward and upward steps correspond to the bead sedimentation and washing, respectively. The signal ΔS_H is proportional to the target concentration. In the inset, the signal arising from the reference sensor is plotted. After the washing steps, the control signal recovers the initial baseline.

gives the signal ΔS_H related to the concentration of target DNA in the sample. As a comparison, the signal arising from the reference sensor, shown in the inset of Fig. 4, recovers the baseline after the washing steps due to the removal of the unbound beads from the sensor surface. A biological signal to background ratio of about 37 is obtained by dividing the ΔS_H signal from the positive and reference sensors, after normalization to the sedimentation signal (ΔS) in order to take into account possible differences in the sensor sensitivities within the same chip. It is worth to note that the sizable signal to noise ratio of Fig. 4 was achieved by choosing the optimum operating point of the sensors according to the proposed criterion. This corresponds to the best detection condition ensuring the lowest limit of detection of the assay.

4. Conclusions

In conclusion, we have shown that the optimum working point for operating a magnetoresistive sensor in order to maximize its sensitivity to the beads does not correspond to the linear part of the $R(H)$ characteristic where the sensitivity to the external field is maximum. The highest sensitivity to beads is instead achieved in the non-linear region, for a specific bias field H_{DC} which allows to maximize the product $\left(\frac{d^2R}{dH^2}\Big|_{H_{DC}} \cdot H_{DC}\right)$. This in turns reflects in the optimization of the sensitivity of the bioassays based on spintronic biosensors, as shown in case of DNA–DNA recognition experiments performed with our MTJ sensors. This work establishes a criterion for choosing the best operating conditions of magnetoresistive sensors for magnetic bead detection and could pave the way to the development of a new generation of sensors properly designed to maximize the bead sensitivity and minimize the limit of detection of related bioassays.

Acknowledgments

This work was funded by Fondazione Cariplo via the project SpinBioMed (Project no. 2008.2330).

Appendix A. Supporting information

Supplementary data associated with this article can be found in the online version at http://dx.doi.org/10.1016/j.bios.2013.03.016.

References

Cardoso, F., 2011. Ph.D. Thesis. Universidade Tecnica de Lisboa, Lisboa.
Chaves, R.C., Bensimon, D., Freitas, P.P., 2011. J. Appl. Phys. 109, 064702.
Donolato, M., Sogne, E., Dalslet, B.T., Cantoni, M., Petti, D., Cao, J., Cardoso, F., Cardoso, S., Freitas, P.P., Hansen, M.F., Bertacco, R., 2011. Appl. Phys. Lett. 98, 073702.
Ferreira, H.A., Feliciano, N., Graham, D.L., Freitas, P.P., 2005. J. Appl. Phys. 97, 10Q904.
Gaster, R.S., Xu, L., Han, S.-J., Wilson, R.J., Hall, D.A., Osterfeld, S.J., Yu, H., Wang, S.X., 2011. Nat. Nanotechnol. 6, 314.
Han, S.-J., Xu, L., Wilson, R.J., Wang, S.X., 2006. IEEE Trans. Magn. 42, 3560.
Hansen, T.B.G., Damsgaard, C.D., Dalslet, B.T., Hansen, M.F., 2010. J. Appl. Phys. 107, 124511.
Lu, Y., Altman, R.A., Marley, A., Rishton, S.A., Trouilloud, P.L., Xiao, G., Gallagher, W.J., Parkin, S.S.P., 1997. Appl. Phys. Lett. 70, 2610.
Martins, V.C., Cardoso, F.A., Germano, J., Cardoso, S., Sousa, L., Piedade, M., Freitas, P.P., Fonseca, L.P., 2009. Biosens. Bioelectron. 24, 2690.
Pirri, G., Damin, F., Chiari, M., Bontempi, E., Depero, L.E., 2004. Anal. Chem. 76, 1352–1358.
Sola, L., Chiari, M., 2012. J. Chromatogr. A 1270, 324–329.
Vavassori, P., Metlushko, V., Ilic, B., Gobbi, M., Donolato, M., Cantoni, M., Bertacco, R., 2008. Appl. Phys. Lett. 93, 203502.
Wang, S.X., Bae, S.-Y., Li, G., Sunc, S., White, R.L., Kemp, J.T., Webb, C.D., 2005. J. Magn. Magn. Mater. 293, 731.
Wiśniowski, P., Almeida, J.M., Cardoso, S., Barradas, N.P., Freitas, P.P., 2008. J. Appl. Phys. 10307A910